Journal of ELECTRONIC MATERIALS, Vol. 44, No. 8, 2015
DOI: 10.1007/s11664-015-3711-y

Dielectric, Ferroelectric, and Piezoelectric Properties of Mn-Doped $K_{0.5}Na_{0.5}NbO_3$ Lead-Free Ceramics

RIGOBERTO LOPEZ-JUAREZ,[1,5] VIRGINIA GOMEZ-VIDALES,[2] M.P. CRUZ,[3] and M.E. VILLAFUERTE-CASTREJON[4]

1.—Unidad Morelia del Instituto de Investigaciones en Materiales, Universidad Nacional Autónoma de México, Antigua Carretera a Pátzcuaro No. 8701, Col. Ex Hacienda de San José de la Huerta, C.P. 58190 Morelia, Michoacán, Mexico. 2.—Instituto de Química, Universidad Nacional Autónoma de México, Circuito Exterior S/N, A.P. 70-360 Mexico, DF, Mexico. 3.—Centro de Nanociencias y Nanotecnología, Universidad Nacional Autónoma de México, A.P. 356, C.P. 22800 Ensenada, BC, Mexico. 4.—Instituto de Investigaciones en Materiales, Universidad Nacional Autónoma de México, Circuito Exterior S/N, A.P. 70-360 Mexico, DF, Mexico. 5.—e-mail: rlopez@iim.unam.mx

In this work, study of manganese-doped potassium-sodium niobate ceramics was performed. It was found that, with increasing Mn^{2+} content from 1 mol.% to 1.5 mol.%, the Q_m changed from 60 to near 500 with no appreciable detriment in piezoelectric properties. These properties first increased with 0.5 mol.%, and remained almost constant with 1 mol.% of manganese. Maximum values for d_{33}, d_{31}, and k_p were 120 pC N^{-1}, 33 pC N^{-1}, and 36%, respectively. Thus, manganese-doped $K_{0.5}Na_{0.5}NbO_3$ ceramics represent an option for high-power applications.

Key words: Ferroelectricity, piezoelectricity, x-ray diffraction, Raman spectroscopy, lead-free ferroelectrics

INTRODUCTION

Research on lead-free piezoelectric ceramics has increased exponentially due to the need to replace toxic lead titanate-zirconate (PZT). These investigations have explored several compounds and their solid solutions, and some of the most studied materials have been $Na_{0.5}Bi_{0.5}TiO_3$ (NBT), $K_{0.5}Na_{0.5}NbO_3$ (KNN), and more recently $Ba_{1-x}Ca_xTi_{1-y}Zr_yO_3$ (BCTZ).[1–4] Among these compounds, NBT has a ferroelectric–antiferroelectric phase transition at relatively low temperature (~200°C), where the piezoelectric response is lost[5] and the piezoelectric properties diminish rapidly. To improve its performance, various additives have been introduced, mainly $BaTiO_3$ and potassium, since it was found that they increase the piezoelectricity by promoting the presence of a polymorphic phase transition near room temperature. Nevertheless, the electromechanical coupling factor (k_p) is still under 37%.[6] In contrast to NBT, BCTZ ceramics have high piezoelectric response, but accompanied with the drawback of a very low Curie temperature (T_C), near 100°C, or even lower depending on their composition.[4] On the other hand, BCTZ does not suffer from element losses during processing, which is common in both KNN and NBT systems. All these drawbacks of NBT and BCTZ make the KNN system and related materials the most desirable choice for many applications.

KNN has high Curie temperature and good piezoelectric properties,[7] but the latter are still low considering the extraordinary piezoelectric properties of PZT. Its crystal structure belongs to the orthorhombic *Bmm2* space group and crystallizes into the perovskite structure (ABO_3). To improve its piezoelectricity, cations such as Li^+, Ta^{5+}, and Sb^{5+} are added into the *A* and *B* sites of the perovskite structure.[8,9] This promotes the change in crystal structure from orthorhombic to tetragonal phase near room temperature [polymorphic phase transition (PPT)], thus enhancing the piezoelectric properties. However, the properties are strongly temperature dependent, which is not desirable for many applications. Regarding some applications,

(Received October 16, 2014; accepted February 21, 2015; published online March 17, 2015)

high power and energy harvesting require materials with hard features, i.e., high Q_m, without detriment to the electromechanical coupling factor or piezoelectric constants d_{33} and d_{31}. The requirement for high mechanical quality factor is because, during operation in high-power applications, mechanical vibrations promote heating and depolarization of ceramics.[10] It has been demonstrated that Cu^{2+}-doped KNN ceramics comply with these requirements, because 1.5% Cu^{2+} doping is sufficient to prepare KNN for power applications. In these ceramics, copper substitutes Nb^{5+} cations, and oxygen vacancies are produced for electroneutrality reasons.[11] Then, it is reasonable to assume that any acceptor cation substituting niobium may induce generation of oxygen vacancies and a hard piezoelectric material as a consequence.

The possible acceptor cations that can be used for preparing hard KNN piezoelectric ceramics include some of the transition metals (Mn^{2+}, Cu^{2+}, Fe^{3+}). In particular, manganese-doped KNN-derived compositions have been prepared and enhanced electrical properties reported.[12,13] In this work, the effects of Mn^{2+} on the structure and dielectric, piezoelectric, and ferroelectric properties of KNN are studied.

EXPERIMENTAL PROCEDURES

Mn^{2+}-doped KNN ceramics ($K_{0.5}Na_{0.5}NbO_3$–xMnO with $0 \le x \le 2$) were prepared by the solid-state method. The raw materials used were K_2CO_3 (99.8%; J.T. Baker), Na_2CO_3 (99.9%; Sigma-Aldrich), MnO (99.9%), and Nb_2O_5 (99.99%; Sigma-Aldrich). First, the carbonates were dried at 200°C for 6 h before weighing and mixed in an agate mortar. The mixture was calcined at 750°C for 1 h and then milled in a conventional ball mill with zirconia medium and alcohol for 12 h. The powders were dried and calcined again at 750°C for 1 h. Before pressing the pellets, MnO was added and ball milled again for 6 h. The pressed samples (13 mm diameter, 3 mm thickness) were sintered at 1100°C for 2 h. The same procedure was applied for preparation of undoped KNN sample; i.e., the two calcinations at 750°C and one milling step for 12 h were performed before sintering.

Structural analysis was performed by x-ray diffraction (XRD) using Cu $K_{\alpha 1}$ radiation (Bruker D8) within a 2θ range of 15–70°; measurements were made on the bulk sintered ceramics (and also on powders during synthesis, not shown here). The microstructure was observed by field-emission scanning electron microscope (Jeol 7600f). The average crystal size was measured on SEM images over more than 100 grains using ImageJ software. For measuring the piezoelectric and dielectric properties, the samples were lapped and silver electrodes deposited on both faces and annealed at 600°C for 30 min. The samples were poled with a direct-current (DC) electric field of 4 kV/mm at 120°C in a silicone oil bath. The piezoelectric constant d_{31} and the electromechanical coupling factor k_p were measured after 24 h of poling with an impedance analyzer (Agilent 4294A) using an iterative method reported elsewhere.[14] The d_{33} piezoelectric constant was measured using the d_{33}-piezometer (APC International). The permittivity was measured at different temperatures (from room temperature to 530°C) and frequencies (1 kHz to 1 MHz). The ferroelectric loops were acquired at room temperature with a Radiant workstation at 100 Hz.

Also, Raman spectroscopy was measured using a Nicolet Almega XR dispersive Raman spectrometer with a Nd:YVO laser (λ = 532 nm). Electron paramagnetic resonance spectroscopy (EPR) measurements were carried out in an EPR spectrometer (Jeol JES-TE300), operated in X-band mode at modulation frequency of 100 kHz with a cylindrical cavity (TE_{011} mode). The samples were measured at room temperature in solid state in a quartz tube (synthetic quartz, Wilmad Glass Company). External calibration of the magnetic field was carried out using a Jeol ES-FC5 precision gaussmeter. Acquisition and manipulation of spectra were performed using the ES-IPRIT/TE program. The EPR parameters were as follows: center field, 335 ± 250 mT; power: 1 mW; microwave frequency, 9.43 GHz; modulation width, 0.1 mT; time constant, 0.1 s; amplitude, 5. In each case, the EPR parameters were held constant.

RESULTS AND DISCUSSION

The x-ray analysis shown in Fig. 1 demonstrated that Mn^{2+} had entered into solid solution, and the structure remained orthorhombic as for undoped KNN. The inclusion of Mn^{2+} into the lattice did not shift the diffraction peaks, only producing some increase in the (211) diffraction line intensity (see the inset). Manganese and niobium have ionic radii of 0.83 Å and 0.64 Å with VI coordination, respectively,[15] whereas those of potassium and sodium are 1.64 Å and 1.39 Å in XII coordination. Thus, it is supposed that Mn^{2+} enters substitutionally into the Nb^{5+} sites (B sites of the perovskite structure). Addition of acceptor ions requires creation of oxygen vacancies to maintain crystal electroneutrality, as in the case of Cu^{2+}-doped KNN, where defect dipoles are formed between oxygen vacancies and Cu^{2+} cations. These dipoles align with the polarization within the ferroelectric domains, pinning the polarization and thus making a hard ferroelectric ceramic. In our case, the formation of defect dipoles $Mn'''_{Nb} - O_v^{\bullet\bullet}$, and the effect on the ferroelectric and piezoelectric properties, are expected to be similar to those in Cu^{2+}-doped KNN.[16]

Creation of oxygen vacancies promotes lattice shrinkage. On the other hand, increasing the Mn^{2+} concentration expands the lattice. The diffraction maxima do not exhibit any considerable change (as seen in Fig. 1), because these two phenomena cancel each other; this has been observed in KNN-derived compositions.[17,18]

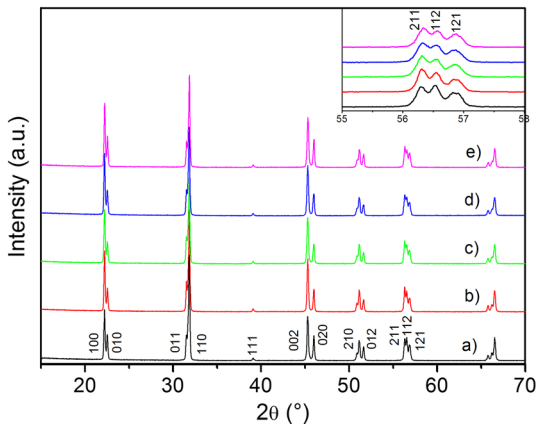

Fig. 1. X-ray diffraction patterns of undoped and Mn^{2+}-doped KNN sintered ceramics: (a) undoped, (b) 0.5 mol.%, (c) 1 mol.%, (d) 1.5 mol.%, and (e) 2 mol.%.

The SEM images of undoped and Mn^{2+}-doped KNN in Fig. 2 show that Mn^{2+} ions promoted crystal growth during sintering. The average grain size of undoped KNN was 1.23 μm, while the samples with 0.5 mol.% to 2 mol.% Mn^{2+} had mean crystal size close to 3.3 μm to 3.8 μm. It is observed that addition of MnO promoted crystal growth. It is reported that, for pure KNN at its optimal sintering conditions, crystals of over 3 μm are found.[3] The enhanced crystal growth is probably due to the formation of liquid phase during sintering, which is formed at high temperature as in Li- and Cu^{2+}-doped KNN ceramics.[16,19] This facilitates matter transport, resulting in larger crystals.

The dielectric permittivity is shown in Fig. 3, where the orthorhombic to tetragonal transition temperature (T_{O-T}) is seen to be close to 210°C, and the tetragonal to cubic transition temperature (T_C)

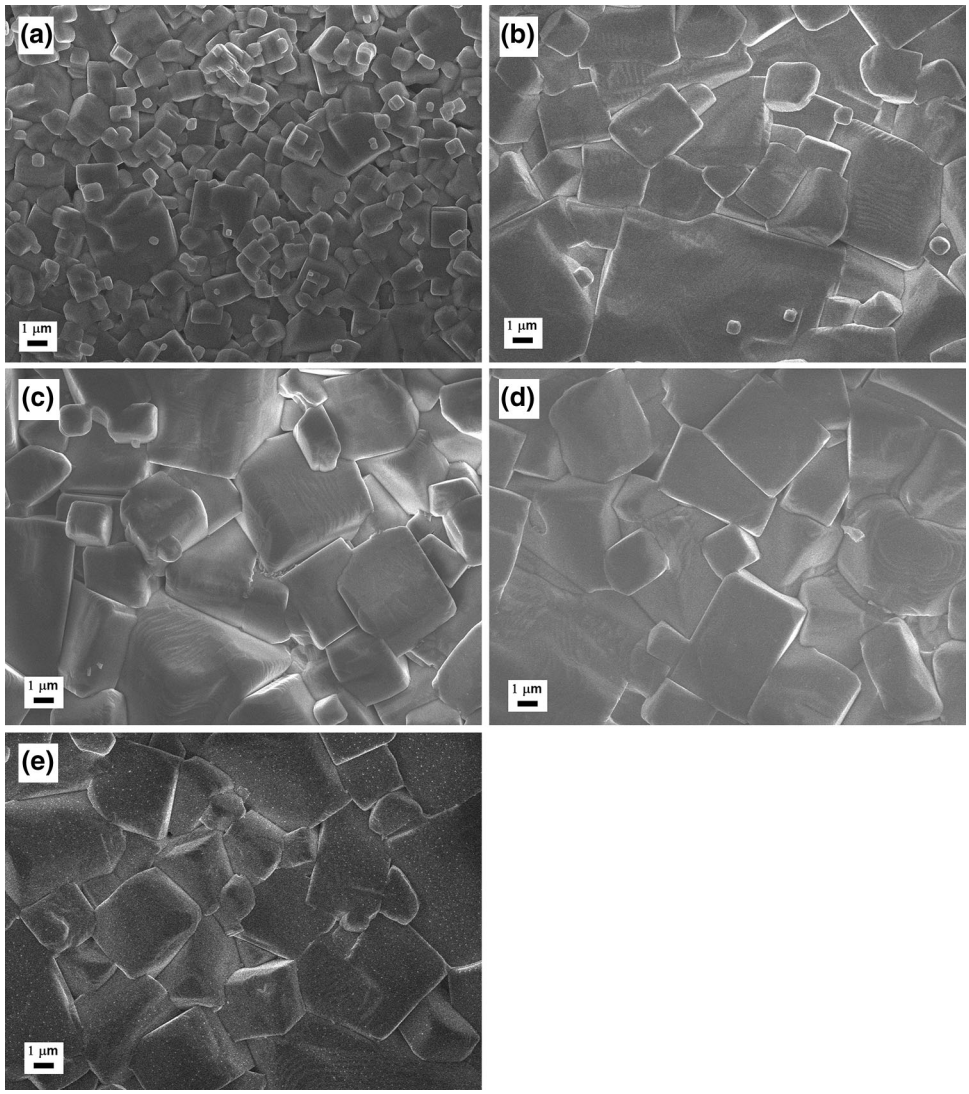

Fig. 2. SEM images of undoped and Mn^{2+}-doped KNN sintered ceramics: (a) undoped, (b) 0.5 mol.%, (c) 1 mol.%, (d) 1.5 mol.%, and (e) 2 mol.%.

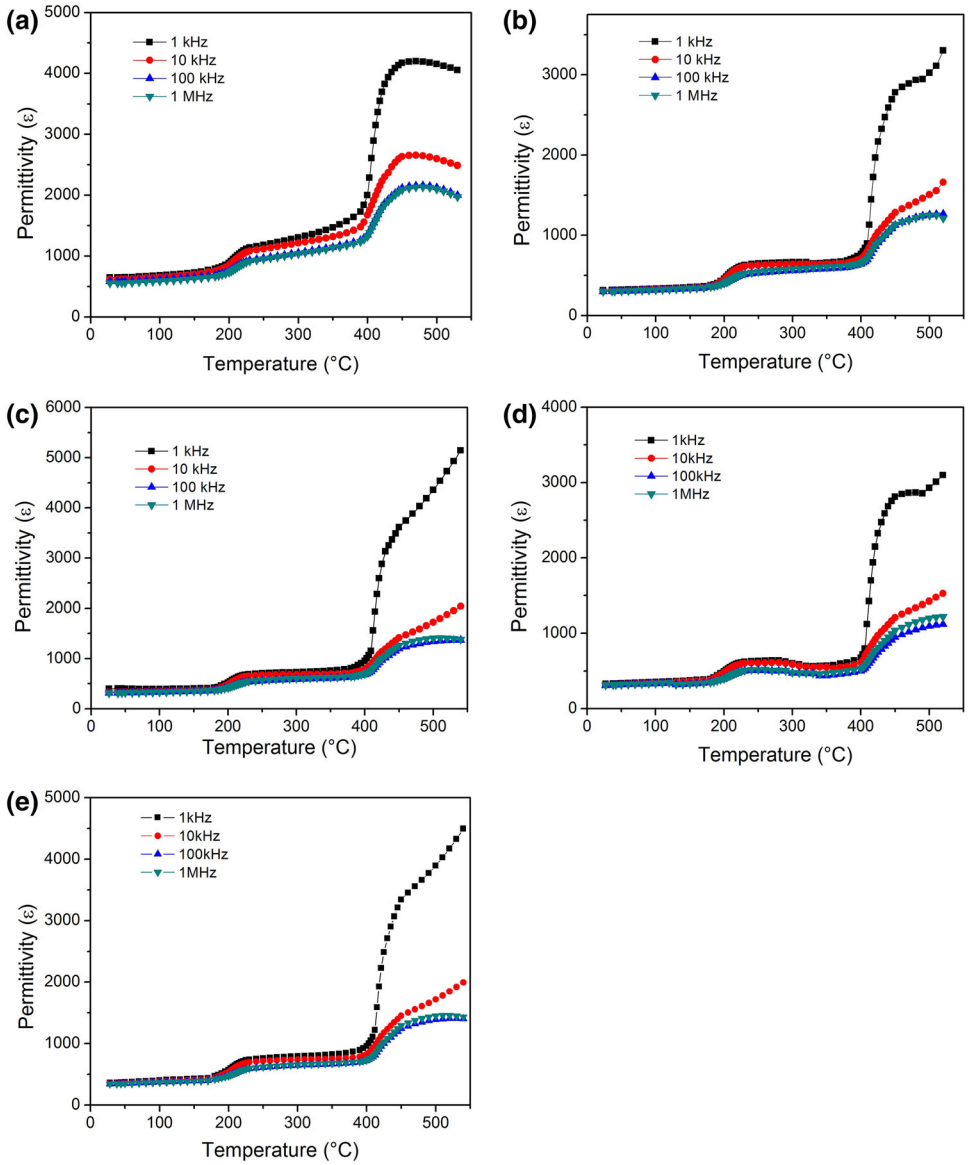

Fig. 3. Dielectric permittivity of undoped and Mn^{2+}-doped KNN sintered ceramics: (a) undoped, (b) 0.5 mol.%, (c) 1 mol.%, (d) 1.5 mol.%, and (e) 2 mol.%.

is over 410°C, as reported for undoped KNN.[3,20] The undoped KNN sample has a "diffuse" phase transition; this is due to the low densification of the sample, as demonstrated by the low k_p and density, as presented below in Table I. It has been stated that the sharpness of the ferroelectric–paraelectric phase transition could be affected by some factors such as porosity and crystal size.[21,22] At temperatures higher than T_C, the dielectric permittivity presents frequency dispersion, which is attributed to the effect of vacancies. This is clearly seen when comparing the undoped sample (Fig. 2a) with the MnO-doped samples (Fig. 2b–e). The oxygen vacancies are responsible for the electrical conduction at high temperatures, and by applying a small alternating-current (AC) field at different frequencies the dispersion of the dielectric constant becomes evident due to the different relaxation time of defects. Furthermore, the relaxation frequency for oxygen vacancy defects is found to lie in the range from kHz to a few MHz.[23] Recently, this kind of anomaly has been observed in perovskite-related materials, being associated with oxygen vacancies and space charge causing defect dipoles.[24,25] In addition, these dielectric anomalies are thermally activated with almost constant activation energy (near 1 eV), and are observed around 400°C to 600°C. In our case, these anomalies are present close to 420°C, matching fairly well with these reports.

Moreover, the magnitude of the dielectric permittivity depends on the polarizability of the ceramics; in this case, the effect of acceptor (Mn^{2+}) doping increases the coercive field of KNN

Table I. Piezoelectric properties of undoped and Mn^{2+}-doped KNN ceramics

Sample	d_{33} (pC N^{-1})	d_{31} (pC N^{-1})	K_p (%)	Q_m	ρ (g/cm^3)
0	110	23	25	60	4.20
0.5	120	33	36	263	4.26
1	112	32	36	313	4.24
1.5	107	31.5	34	471	4.25
2	94	26	29	316	4.27

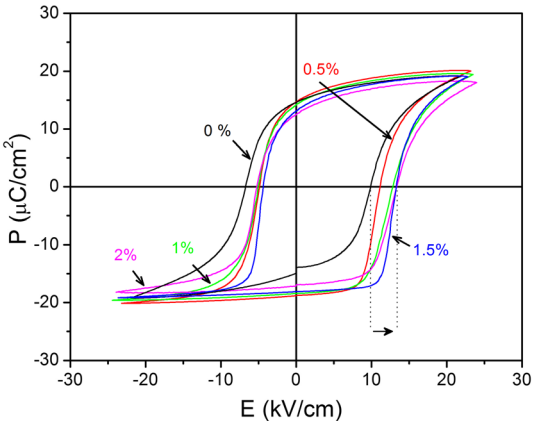

Fig. 4. Ferroelectric hysteresis loops of sintered ceramics.

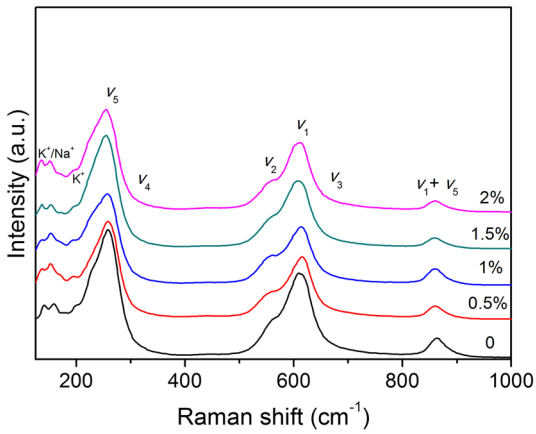

Fig. 5. Raman spectra of sintered ceramics.

ferroelectric ceramics, decreasing the polarizability and thus leading to the low permittivity at room temperature as observed in Fig. 3.

This can be further confirmed in Fig. 4, where the ferroelectric loops are shown. As can be seen from these, an electric bias field is present in Mn^{2+}-doped ceramics as compared with the undoped sample, where no bias field exists, and it increases as the Mn^{2+} concentration increases (marked with an arrow in Fig. 4). This increment in the bias field is due to the higher concentration of oxygen vacancies as the Mn^{2+} concentration increases, and more defect dipoles enhance the pinning of the polarization. Moreover, samples with higher Mn^{2+} doping level show lower remnant polarization, as expected because of the higher level of defect dipoles. Only heating the materials at temperatures surpassing T_C will reorient them within the bulk material. The ferroelectric loops of Mn^{2+}-doped KNN are characteristic of hard ferroelectric materials, and have also been reported for CuO-doped KNN with double defect dipole which enhances the bias field.[26]

Table I presents the piezoelectric properties of the Mn^{2+}-doped KNN ceramics: d_{33}, d_{31}, and k_p increase for the 0.5 mol.% Mn^{2+}-doped ceramic when compared with undoped KNN. With increasing doping level, the piezoelectric properties remain almost constant, and only the presence of 2 mol.% manganese induces a considerable drop in these properties. However, the mechanical quality factor Q_m does not follow the same trend as all the piezoelectric properties.

The highest Q_m value was for the sample with 1.5 mol.%, as can be seen from the hysteresis loops. It is evident that the 1.5 mol.% sample has slightly lower coercive field than the 2 mol.% sample. The Q_m is related with domain-wall motion (90° mainly), microstructure, and electrical conductivity.[12,17,18] So, as the Mn^{2+} concentration increases, the amount of electrical dipoles which pin the polarization also increases, as does Q_m accordingly, reaching a maximum value at $x = 1.5$. Q_m decreases for $x = 2$ because the densification decreases, which also influences this property as stated above.

On comparing the piezoelectric properties with some reports on copper- and manganese-doped KNN ceramics, it is observed that k_p, d_{33}, and Q_m are of the same order, being only sometimes slightly higher or lower.[11,12,19,27] In general, it is difficult to find high values of all these properties for one particular composition of lead-free piezoelectric ceramic; it is more common for the maximum mechanical quality factor to be accompanied by moderate k_p and d_{33} or vice versa.

The Raman spectra are shown in Fig. 5. The spectra are typical of KNN ceramics,[28] with stretching (ν_1, ν_2, ν_3) and bending (ν_4, ν_5, ν_6) modes of NbO_6 octahedra merging between 200 cm^{-1} and 900 cm^{-1}, whereas the translational and rotational modes of K^+/Na^+ and NbO_6 octahedra appear below

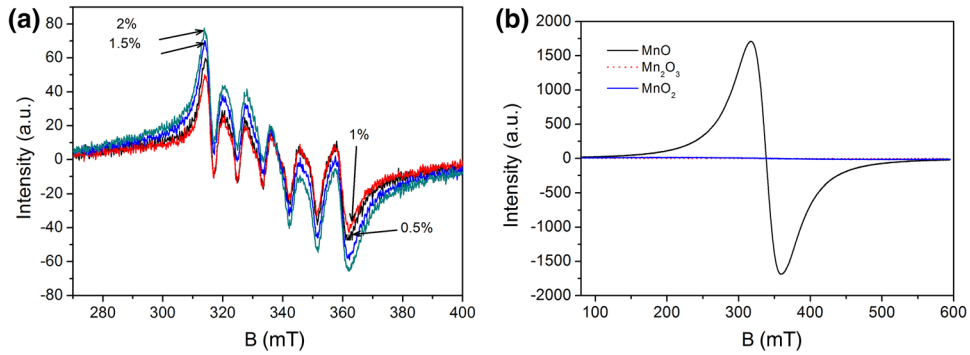

Fig. 6. EPR spectra of (a) Mn^{2+}-doped KNN ceramics and (b) manganese oxides.

200 cm^{-1}. It is worth noting the decrease in intensity, mainly in the v_1 and $v_1 + v_5$ modes, occurring with the increase in Mn^{2+} doping. This may be related to softening of these modes, because of manganese replacement of niobium, and the creation of oxygen vacancies, which influence the vibrational modes of the modified niobium–oxygen or manganese–oxygen octahedra.

Finally, the electron paramagnetic resonance spectroscopy results are given in Fig. 6, showing a signal in the center field due to the electronic transition (+1/2, −1/2) with $g = 2.01$ and the interaction with the nuclear spin of manganese $I_{Mn} = 5/2$, clearly showing the sextet characteristic of Mn^{2+} cation with hyperfine coupling constant of $A = 8.82$ mT.[29] Furthermore, the most stable oxidation state of manganese is 2+ ($S = 1/2$). The spectra corresponding to the manganese oxides are presented in Fig. 6b. There is a clear difference in the signal between MnO versus Mn_2O_3 and MnO_2; MnO shows an intense, isotropic signal with $g = 2$, due to the (+1/2, −1/2) electronic transition, whereas resonance due to Mn_2O_3 and MnO_2 was barely present under these measurement conditions. Moreover, it was evidenced that, when MnO_2 (Mn^{4+}) was added to $BaTiO_3$-doped $Bi_{0.5}Na_{0.5}TiO_3$ ceramics, the manganese ion was reduced to Mn^{2+} and Mn^{3+}.[30] Thus, further oxidation of manganese under the sintering conditions used in this work is not plausible.

CONCLUSIONS

Manganese-doped KNN ceramics showed good piezoelectric properties. The Mn^{2+} cation entered into the solid solution, creating oxygen vacancies and thereby hardening the ferroelectric properties, as evidenced by the ferroelectric loops. The mechanical quality factor was enhanced, while all the piezoelectric properties remained almost constant. Raman spectroscopy also demonstrated the existence of oxygen vacancies, resulting in a drop in intensity for some vibrational modes. Electron paramagnetic resonance proved the 2+ oxidation state of manganese cations. The mechanical quality factor increased almost tenfold as compared with undoped KNN. So, Mn^{2+}-doped KNN piezoceramics are promising for power applications, such as piezoelectric transformers.

ACKNOWLEDGEMENTS

Special thanks are due to CONACyT-México for financial support under project CB-2011-1 No. 166108. The authors wish to thank Omar Novelo and Adriana Tejeda for SEM and XRD analysis.

REFERENCES

1. V.A. Isupov, *Ferroelectrics* 315, 123 (2005).
2. A. Chowdhury, J. Bould, Y. Zhang, C. James, and S.J. Milne, *J. Nanopart. Res.* 12, 209 (2010).
3. R. López, F. González, M.P. Cruz, and M.E. Villafuerte-Castrejón, *Mater. Res. Bull.* 46, 70 (2011).
4. W. Liu and X. Ren, *Phys. Rev. Lett.* 103, 257602 (2009).
5. R. López-Juárez, R. Castañeda-Guzmán, F. Rubio-Marcos, M.E. Villafuerte-Castrejón, E. Barrera-Calva, and F. González, *Dalton Trans.* 42, 6879 (2013).
6. C. Xu, D. Lin, and K.W. Kwok, *Solid State Sci.* 10, 934 (2008).
7. D.W. Baker, P.A. Thomas, N. Zhang, and A.M. Glazer, *Appl. Phys. Lett.* 95, 091903 (2009).
8. X. Sun, J. Deng, J. Chen, C. Sun, and X. Xing, *J. Am. Ceram. Soc.* 92, 3033 (2009).
9. P. Zhao, B.P. Zhang, R. Tu, and T. Goto, *J. Am. Ceram. Soc.* 91, 3078 (2008).
10. E. Li, H. Kakemoto, S. Wada, and T. Tsurumi, *IEEE T. Ultrason. Ferr.* 55, 980 (2008).
11. E.M. Alkoy and M. Papila, *Ceram. Int.* 36, 1921 (2010).
12. X.P. Jiang, Y. Chen, K.H. Lam, S.H. Choy, and J. Wang, *J. Alloy. Compd.* 506, 323 (2010).
13. S.Y. Lee, C.W. Ahn, A. Ullah, H.J. Seog, J.S. Kim, S.H. Bae, and I.W. Kim, *Curr. Appl. Phys.* 11, S266 (2011).
14. C. Alemany, A.M. González, L. Pardo, B. Jiménez, F. Carmona, and J. Mendiola, *J. Phys. D Appl. Phys.* 28, 945 (1995).
15. R.D. Shannon, *Acta Crystallogr. A* 32, 751–767 (1976).
16. H.-C. Song, K.-H. Cho, H.-Y. Park, C.-W. Ahn, S. Nahm, K. Uchino, S.-H. Park, and H.-G. Lee, *J. Am. Ceram. Soc.* 90, 1812–1816 (2007).
17. W.-F. Liang, D.-Q. Xiao, J.-G. Wu, W.-J. Wu, and J.-G. Zhu, *Front. Mater. Sci.* 8, 165 (2014).
18. D. Lin, Q. Zheng, K.W. Kwok, C. Xu, and C. Yang, *J. Mater. Sci* 21, 649 (2010).
19. H.-Y. Park, C.-W. Ahn, K.-H. Cho, S. Nahm, H.-G. Lee, H.-W. Kang, D.-H. Kim, and K.-S. Park, *J. Am. Ceram. Soc.* 90, 4066–4069 (2007).
20. L. Wu, J.L. Zhang, C.L. Wang, and J.C. Li, *J. Appl. Phys.* 103, 084116 (2008).

21. F.D. Morrison, D.C. Sinclair, and A.R. West, *J. Appl. Phys.* 86, 6355 (1999).
22. T.-T. Fang, H.-L. Hsieh, and F.-S. Shiau, *J. Am. Ceram. Soc.* 76, 1205 (1993).
23. C. Elissalde and J. Ravez, *J. Mater. Chem.* 11, 1957–1967 (2001).
24. Z. Meini, X. Kebiao, W. Guojing, and W. Chunchang, *Chin. Sci. Bull.* 58, 713 (2013).
25. T.-F. Zhang, X.-G. Tang, Q.-X. Liu, S.-G. Lu, Y.-P. Jiang, X.-X. Huang, and Q.-F. Zhou, *AIP Adv.* 4, 107141 (2014).
26. S.M. Ke, H.T. Huang, H.Q. Fan, H.K. Lee, L.M. Zhou, and Y.W. Mai, *Appl. Phys. Lett.* 10, 082901 (2012).
27. D. Lin, M.S. Guo, K.H. Lam, K.W. Kwok, and H.L.W. Chan, *Smart Mater. Struct.* 17, 035002 (2008).
28. K. Kakimoto, K. Akao, Y. Guo, and H. Ohsato, *Jpn. J. Appl. Phys.* 44, 7064 (2005).
29. Y. Kizaki, Y. Noguchi, and M. Miyayama, *Appl. Phys. Lett.* 89, 142910 (2006).
30. E. Erdem, S. Schaab, W. Jo, A. Ozarowski, J. Van Tol, and R.A. Eichel, *Ferroelectrics* 428, 116 (2012).